This document is the Accepted Manuscript version of a Published Work that appeared in final form in ACS Applied Materials & Interfaces, copyright © American Chemical Society after technical editing by the publisher.

To access the final edited and published work see: http://pubs.acs.org/articlesonrequest/AOR-i6TdigYxv3HhPqUV6u3s

Block copolymer patterning for creating porous silicon thin films with tunable refractive indices

Hanna H. Hulkkonen*, Turkka Salminen, and Tapio Niemi

Optoelectronics Research Centre, Tampere University of Technology, Korkeakoulunkatu 3, 33720 Tampere, Finland

ABSTRACT

We investigated the use of block copolymer self-assembly for tuning the optical properties of silicon. We fabricated porous silicon by etching a hexagonally ordered pore pattern onto the surface of silicon wafers using poly(styrene-2-vinylpyridine) to prepare the etch mask. Contrary to typical block copolymer lithography, we did not need to use a range of different polymers to vary the pore size. We used the dry etching time as a way to increase the pore diameter and thus the porosity. The optical properties of the fabricated porous thin films were characterized by two effective medium approximations. Both the Volume Averaging Theory and the 2D Maxwell–Garnett Theory gave similar effective refractive index values, although the latter was more accurate in predicting the film porosity. The refractive indices of the produced thin films could be varied by controlling the porosity. A maximum decrease of 30 % in the refractive index was observed at 34 % porosity compared to bulk silicon. We also demonstrated over 60 % decrease in the reflectance of silicon at 500 nm wavelength. The presented block copolymer method can be used to tailor semiconductor and dielectric layers for photonic

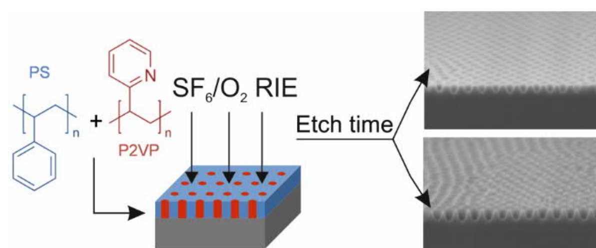

applications without the size limitations of conventional lithography or the unpredictability of other pore-forming fabrication methods.

KEYWORDS: Block copolymer, nanolithography, porous silicon, tunable refractive index, effective medium approximation

INTRODUCTION

Block copolymers (BCPs) have been of interest in the fabrication of porous media due to their ability to self-assemble into highly ordered periodic structures. The cylindrical morphology is of particular interest since it allows the minor domain to be selectively removed to form an organized array of evenly-sized holes. The size of the holes is usually controlled by selecting a BCP with the appropriate molecular weight. Subtle changes to the polymer microdomain size can be done by blending in homopolymers that segregate to the cylindrical domains and enlarge their size.[1] The domain removal conditions can also affect the size of the fabricated pores as shown by Yin et al. in a study that used selective swelling of one polymer domain at varying temperatures.[2] The method used for domain removal depends on the block copolymer chemistry and includes processes such as selective swelling,[2] ozonolysis,[3] or degradation by UV-irradiation followed by solvent treatment.[4] The versatility of block copolymers has made them desirable tools to produce precisely tailored nanoporous materials that can be of use in multiple applications including filtration,[5] catalysis[6] and nanolithography.[7]

Lithographic patterning of semiconductors using BCPs was demonstrated already early on by Park et al.[3] Since then, BCPs have proven to be very useful as templates for fabricating dense arrays of dot and line patterns, and more recently also gyroidal structures with unique optical properties.[8] The BCP pattern is transferred onto the underlying substrate either by etching or by using the BCP as a template for material deposition. Typical block copolymers are not very resistant to etching methods so successful pattern transfer may be problematic. A comprehensive review by Cummins et al. lists various strategies including sequential infiltration synthesis, atomic layer deposition and metal evaporation that can be used to incorporate inorganic materials into BCP films and enhance the durability of the BCP etch masks.[9] Etch resistant BCP patterns can

also be made directly using polymers where one block contains inorganic moieties such as in polydimethylsiloxane (PDMS), which forms a durable silicon oxide hard mask after oxidization. However, we are more interested in BCPs containing a multipurpose polyvinylpyridine (PVP) block that can be either bonded with etch contrast agents or selectively removed without etching. For the mask to function correctly, the BCP features have to be oriented perpendicular to the substrate surface. The orientation and alignment of cylindrical domains have been extensively studied using neutral brush layers,[10] topographic confinement,[11] electrical fields[12] and solvent evaporation treatments.[13]

The incorporation of holes into a bulk semiconductor significantly affects the optical and electrical properties of the material. The porous thin film is considered a nanocomposite consisting of a solid matrix with nanoscale inclusions of air. The size of the inclusions must be much smaller than the wavelength of light so that the light only experiences the collective response of the composite material and not that of the individual structures. Gases, such as air, have very low refractive indices due to their low density. The addition of air effectively reduces the refractive index of the porous material. The effective electromagnetic properties of nanoporous materials can be described using numerous effective medium approximations (EMAs). Some of the most common EMAs are the Maxwell–Garnett theory, Bruggeman's model, Lorentz-Lorenz equation and the Volume Averaging Theory.[14] Most EMAs have been derived for certain nanocomposite architectures and measuring arrangements. Owing to the amount of models available and their validity limitations there is some uncertainty on what models to use when describing nanoporous materials. A study by Braun and Pilon concluded that for cylindrically-shaped pores the effective optical properties could be calculated based solely on the porosity and that film thickness, pore shape and distribution were insignificant.[15] We observed based on experimental and theoretical works[14–17] that depending on the optical measurement setup and the light polarization the effective refractive index predictions that best complied with porous silicon were achieved using either the Volume Averaging Theory (VAT) or the 2D Maxwell–Garnett Theory (2D MGT). The VAT assumes arbitrarily shaped and distributed inclusions while the 2D MGT is derived for films with monodisperse, cylindrical inclusions.[14,17]

Porous silicon thin films have found use as refractive index-tailored waveguides, antireflection coatings, Bragg reflectors and biosensors due to their tunable properties and the ease of integration

into semiconductor device fabrication. The effective properties can be controlled by altering the degree of porosity but the typical porous silicon fabrication methods produce somewhat unpredictable pore structures. Porous silicon has typically been fabricated by electrochemical anodization of doped Si in solutions containing hydrofluoric acid. The resultant pore structure and size distribution depend on processing conditions such as the current density, electrolyte concentration, substrate doping, etch time and temperature.[18]

Here we demonstrate a straightforward way to fabricate silicon thin films with controlled porosity and a highly organized pore structure using poly(styrene-2-vinylpyridine) block copolymer lithography. We characterize the fabricated porous thin films using spectrophotometry with TE-polarized light and estimate the optical properties of the porous films using the VAT and the 2D MGT.

EXPERIMENTAL SECTION

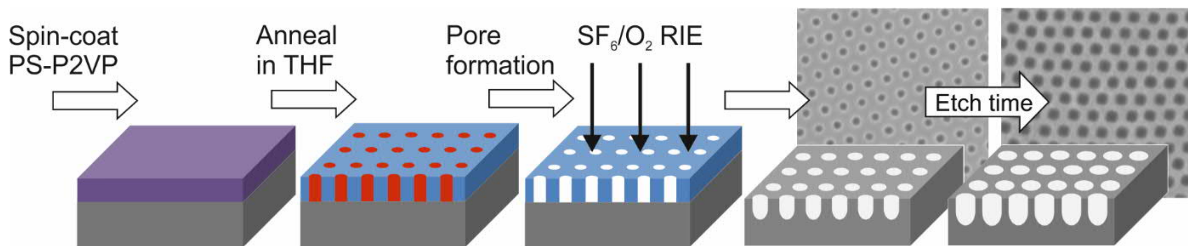

Figure 1. Experimental procedure for preparing porous thin film masks from PS-P2VP and controlling the porosity of silicon by reactive-ion etching.

Materials. The asymmetrical block copolymer poly(styrene-2-vinylpyridine) (PS-P2VP) (M_n= 135-b-53 kg/mol, PDI = 1.18) was purchased from Polymer Source Inc. and was used as received without purification. Anhydrous toluene and tetrahydrofuran (THF) were purchased from Sigma-Aldrich. Commercial, laboratory-grade 2-propanol and ethanol were also used.

Fabrication of BCP mask. Silicon wafers were cleaned with 2-propanol and used with the native oxide layer intact. Due to the relatively high molecular weight of the PS-P2VP, the polymer

was dissolved in a 70:30 mixture of toluene and THF and stirred for over 12 hours to ensure complete dissolution. A 1–1.5 w/v-% solution was spin-coated onto the substrates at 3000 rpm for 60s. We used a closed chamber SSE OPTIcoat spinner for better film uniformity. Samples were immediately baked on a hotplate at 125 °C for 2 minutes followed by controlled solvent vapor annealing in THF for 5 to 10 minutes. The PS-P2VP created a hexagonally arranged dot pattern with an average center-to-center distance of 74 nm.

Silicon etching using BCP mask. To fabricate the nanoporous template the P2VP domains were selectively swelled and made to collapse creating cylindrical, perpendicularly oriented pores. Selective swelling was done by immersing the samples in ethanol at room temperature for 30 minutes, after which the samples were blow-dried with nitrogen. The highly ordered porous templates were then used as dry etch masks without further treatment. Dry etching of silicon was carried out using reactive ion etching in SF_6/O_2 plasma with either 80 W or 160 W RF power (12/9 sccm, 30 mTorr pressure, Oxford Plasmalab System100). We investigated the effect of different etching times on the pattern transfer. After silicon etching, polymer residues were removed during a brief O_2 plasma treatment (30 sccm, 100 W RF power, 100 mTorr pressure). The workflow of the BCP nanopatterning process is illustrated in Fig. 1.

Film characterization. The surface morphologies of the annealed BCP thin films and the etched silicon wafers were examined using a field emission scanning electron microscope (Zeiss Ultra 55) with 0.8–3 kV acceleration voltage. For quality control, the thickness of the BCP masks was determined using a laser ellipsometer (Rudolph Research AutoEL III) with a HeNe laser at a 70° incident angle. Porosity and pore size analysis was performed on 3.8 x 2.85 µm SEM images using Fiji, an open source scientific image processing software based on ImageJ. Automatic image thresholding was used to minimize user-bias and a particle analysis tool was used to calculate the porosity, average pore size and standard deviation from the converted binary images.

Optical measurements. Reflectance of the etched silicon wafers was measured using a Perkin Elmer Lambda 1050 spectrophotometer with a universal reflectance accessory. We used an incident angle of 8 degrees, a rectangular beam shape with an area of 5 x 5 mm^2 and TE-polarization where the electric field vector is perpendicular to the cylinders. The reflectance data was fitted to a model consisting of a bulk silicon substrate and a layer with an effective refractive

index determined by the layer porosity. Fitting was done using a transfer-matrix method that used the volume fraction of air f_v and film thickness h as fitting parameters.[19]

The effective refractive index was determined by applying the VAT and the 2D MGT[14] and utilizing refractive index values for bulk silicon and air.[20] These theories approximate the complex refractive index where the real part n is the refractive index and the imaginary part k is the extinction coefficient of the nanocomposite thin film. The complex effective refractive index $(n_{eff} - jk_{eff})$ given by the VAT is defined by:

$$n_{eff}{}^2 = \frac{1}{2}\left[A + \sqrt{A^2 + B^2}\right] \quad (1)$$

$$k_{eff}{}^2 = \frac{1}{2}\left[-A + \sqrt{A^2 + B^2}\right] \quad (2)$$

where $A = f_v(n_{air}{}^2) + (1 - f_v)(n_{Si}{}^2 - k_{Si}{}^2)$ and $B = 2n_{Si}k_{Si}(1 - f_v)$

and by the 2D MGT it is:

$$(n_{eff} - jk_{eff})^2 = n_c{}^2\left[1 - \frac{2f_v(n_c{}^2 - n_i{}^2)}{n_c{}^2 + n_i{}^2 + f_v(n_c{}^2 - n_i{}^2)}\right] \quad (3)$$

The complex notations $n_c = (n_{Si} - jk_{Si})$ and $n_i = (n_{air} - jk_{air}) = n_{air}$ contain the refractive indices and extinction coefficients of silicon (subscript "Si") and air (subscript "air"). The volume fraction (porosity) of air in the thin film is denoted f_v.

RESULTS AND DISCUSSION

The PS-P2VP was spin-coated onto solvent-cleaned silicon wafers resulting in polymer films with an initially disorganized morphology and a film thickness of 43–55 nm. The BCP films were subjected to controlled solvent vapor flow annealing using a metal chamber and a N_2–bubbler system similar to the one presented by Jin et al.[21] Perpendicular orientation of the P2VP cylinders was achieved by annealing in THF for 10 minutes followed by fast quenching.

The selective swelling of P2VP in room temperature ethanol for 30 min produced an open-pore polymer mask with an estimated hole diameter of 27 nm. The prevailing theory explaining the

pore formation in PS-P2VP is that due to the constriction of the PS matrix the selective solvent swells the P2VP chains up and out from the cylinders and after drying the chains collapse onto the film surface and the pore walls.[2] The holes in our BCP films were spatially arranged in a highly ordered hexagonal pattern in similarly oriented grains (grain diam. 1 μm or larger) that covered the whole substrate surface. No dewetting was observed on the 1 cm^2 and 4 cm^2 wafer pieces. The mask fabrication could easily be scaled up to larger wafers and the main limiting factor is the solvent annealing chamber that currently fits a maximum wafer size of 2 inches.

We were able to fabricate silicon thin films with increasing pore sizes without having to use a wide range of BCPs with different molecular weights. The silicon thin films with pore diameters ranging from 26 to 58 nm were all created using a single polymer and an etch mask that always had the same initial hole diameter (approx. 27 nm). The change in pore size arose from the tuning of the dry etching time, which was varied from 15 s to a maximum of 50 s. The gradual lateral etching of the BCP mask widened the hole openings, which resulted in larger pores etched into silicon until neighboring pores began to limit the growth. The lateral widening was more apparent after longer etching times as seen in Table 1. In addition to variations in pore width also the pore depth varied with etch time from 42 to a maximum of 60 nm for lightly etched samples (Fig. 2A-B). A loss of pore depth and a change in the pore profile was observed after longer etching times, which was likely a result of etching away first the BCP mask and then the cylinder structures (Fig. 2C). We also tried using a lower RF power of 80 W instead of 160 W but the etch was too isotropic and did not produce clear pore structures.

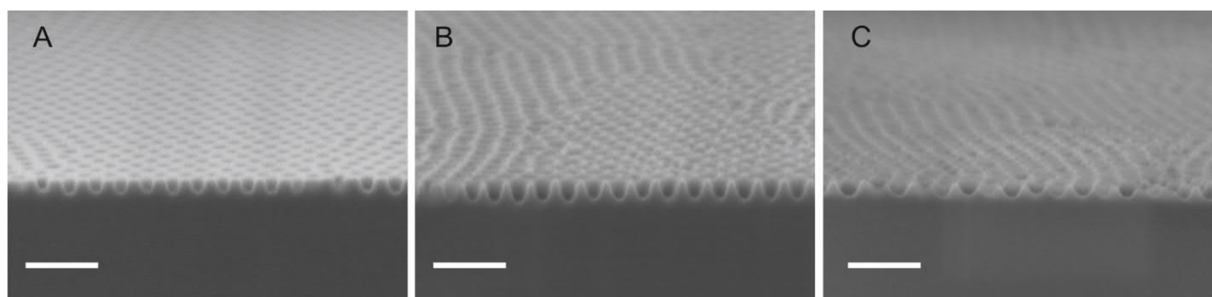

Figure 2. Etch profile of porous silicon thin films with A) 15 s, B) 20 s and C) 40 s of etching in SF_6/O_2 RIE. A lateral widening of the pores is seen and over-etching is apparent after longer etching times. Scale bars 200 nm.

Optical characterization. The progressive increase in the pore diameter resulted in an increase in the film porosity as calculated by image analysis. All porous thin films displayed a decrease in measured reflectance compared to bare silicon (Fig. 3). Furthermore, the decrease in the overall reflectance at 500–900 nm was observed to follow the increase in film porosity up to a point (Fig. 3A-D). A visible color change was observed in the samples starting from a light blue tint and reaching a dark blue color at approximately 34 % porosity (pore diam. 45 nm). The dark blue colored films also had the lowest reflectance with a maximum 62 % decrease in reflectance at 500 nm wavelength.

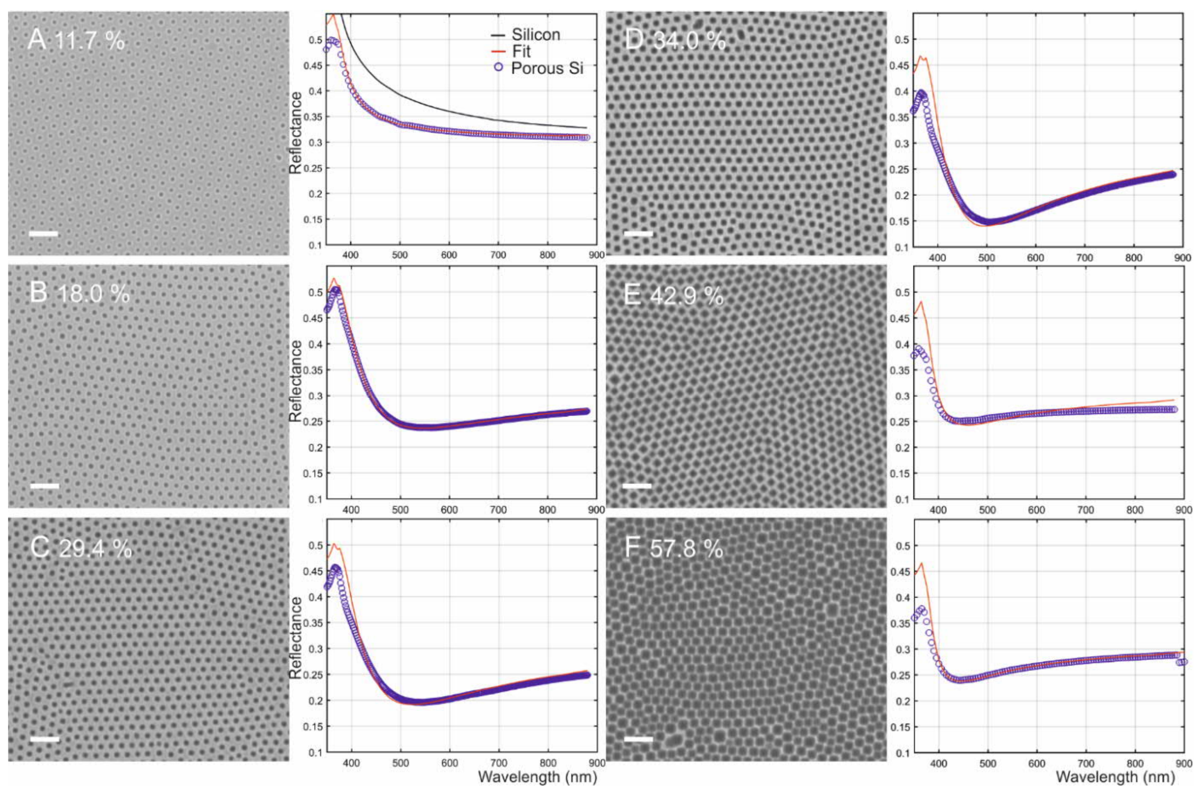

Figure 3. SEM images and measured reflectance spectra from porous silicon thin films with porosities A) 11.7 % B) 18.0 % C) 29.4 % D) 34.0 % E) 42.9 % and F) 57.8 %. The reflectance of all porous films (blue) differed from the bare silicon reference (A, black). Reflectance was also modelled (red) using porosity f_v and thickness h as fitting parameters. Scale bars 200 nm.

However, thin films with over 40 % estimated porosity did not follow the trend in decreasing reflectance and a relapse of the reflectance towards that of pure silicon was seen (Fig. 3E-F). This behavior can be explained by examining the cross-sections of the porous thin films. The thin films that appear to have a high porosity in top-down SEM images have actually lost the cylindrical pore

shape and only have very shallow (25–35 nm) spherical indentations due to mask erosion and over-etching (Fig. 2C). Therefore, surface image analysis did not give a realistic approximation of the porosity for these thin films. Since the actual film porosity was lower than estimated, the overall decrease in reflectance was not as large as was expected.

To further study the optical properties of the thin films they were modelled as homogenous layers with a thickness h and an air volume fraction f_v according to the VAT and the 2D MGT. The fitted reflectance models agreed very well with the measurement data as seen in Fig 3 (2D MGT fit displayed). Both the VAT and the 2D MGT models produced similar fits with a maximum difference of 0.8 %. There is a discrepancy between the measured and the modelled reflectance in the ultraviolet region and the effect is more pronounced as the pore size grows. At shorter wavelengths, the pores are likely becoming too large to be considered sub-wavelength nanostructures for modelling using the effective medium approach. Similarly, Pap et al. observed a difference between the experimental and theoretical reflectance and attributed it to enhanced Rayleigh scattering from the pores at short wavelengths.[16] The effective medium approximations do not account for the intensity loss caused by scattering.

Table 1. Characteristics of porous thin films based on SEM image analysis and model fitting

	IMAGE ANALYSIS		**MODELLING**		
Etch time [s]	Pore diam. [nm]	Porosity [%]	2D MGT f_v [%]	VAT f_v [%]	h [nm]
15	26.2 ± 1.9	11.7	11.9	20.7	21
20	30.5 ± 2.1	17.1	19.2	31.3	30
15	31.6 ± 1.6	18.0	22.0	35.0	34
20	40.9 ± 2.8	29.4	29.2	44.1	36
20	44.8 ± 2.6	34.0	38.4	54.5	38
40	49.2 ± 3.5	42.9	29.3	44.0	26
30	57.6 ± 6.4	57.8	31.8	47.4	25

f_v = volume fraction of air, h = modelled layer thickness

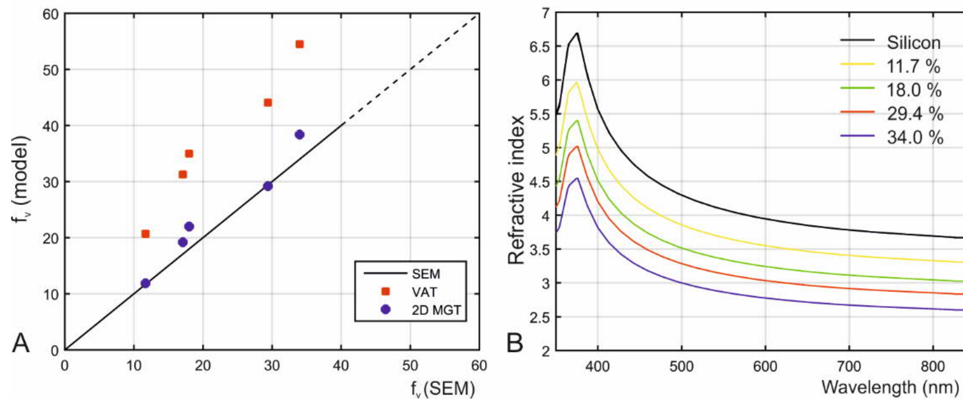

Figure 4. A) Comparison of porosity values acquired via data fitting of the VAT and the 2D MGT. The line labeled 'SEM' is a guide to the eye. B) Effective refractive indices of porous silicon calculated by fitting the 2D MGT of the thin films to the optical reflectance.

The 2D MGT was accurate in calculating the volume fraction f_v of the cylindrically porous thin films under 40 % porosity (Fig. 4A). The volume fraction f_v ranging from 11.9 to 38.4 was observed to correspond to porosity values 11.7–34.0 % estimated via SEM image analysis. The small variations between the measured and modelled porosities can be attributed to uncertainties in the image analysis method. The VAT was not as effective in calculating the porosity and it overestimated the film porosity in increasing amounts (Fig. 4A). The differences between the two models arise from the differing assumptions concerning the pore structure. Another concern is that the measurement configuration and light polarization affect the reflectance and the predicted properties of cylindrically porous films due to the anisotropy of the thin films.[14] Here we note that when using light polarization where the electric field vector is perpendicular to the cylinders the 2D MGT has better predictive power. The estimated pore size, the porosity of the thin films, as well as the 2D MGT and VAT fitting parameters, are summarized in Table 1.

For over-etched films (diam. > 49 nm, porosity > 40 %) both models computed a decreased optical thickness and a reduced volume fraction. Since the profile of the pores changed during over-etching, the reliability of the EMAs is questionable. For example, the 2D MGT model is derived for cylindrical inclusions and it will likely not give reliable predictions concerning the physical and optical properties of films with spherical indentations. We think that the simple effective medium approximations for a single thin film layer are not appropriate for comparing samples with different 3D architectures.

Despite their differences in interpreting the volume fraction, both effective medium approximations gave acceptable predictions concerning the complex refractive indices. The relative differences between the indices given by the two models were under 0.5 %. The extinction coefficient k showed little change as a result of increased porosity (Fig. S1, S2). However, at short wavelengths scattering and pore size related losses likely caused aberrations to the models. In principle, most EMAs have been developed for estimating the real part of the effective refractive index. Nevertheless, the imaginary part can also be estimated with some restrictions as proposed by Hutchinson et al.[14]

A gradual decrease in the effective refractive index was observed in cylindrically porous silicon thin films as shown in Fig. 4B. The lowest refractive index was achieved with a surface porosity of 34 % and the thin film displayed a 30 % change compared to bulk silicon. Low-index materials are particularly desirable in broadband antireflection coatings and optical devices that require a high-index contrast such as waveguides and microresonators.[22] Solid, naturally occurring semiconductor materials with indices smaller than 1.4 do not really exist. Extremely low-index semiconductors could be realized by selecting substrate materials that already have a low refractive index and incorporating air-filled pores onto the substrate surface using block copolymer lithography. The fact that the substrate and the porous surface layer are both from the same material reduces the processing steps needed and is an advantage in semiconductor device fabrication.

CONCLUSIONS

In conclusion, we have demonstrated that the optical properties of silicon can be tuned using a simple process of block copolymer lithography. First, arrays of perpendicularly oriented cylinders were obtained with a brief solvent vapor treatment, where no substrate surface modifications or neutral layers were needed. Secondly, etch masks were formed by selective removal of one BCP component and the resulting hole structure was transferred into silicon using SF_6/O_2 etching. The etched pore structure was spatially highly ordered and uniform over the whole wafer surface. The diameter of the pores and hence the porosity of silicon could be increased with etching time up to a point where the neighboring pores began to limit the growth. The method presented here allows a broad porosity range to be reached with a single block copolymer. The molecular weight of the selected BCP determines the periodicity of the pores and sets the minimum accessible pore size.

The effective refractive indices of porous silicon thin films could be determined by fitting either 2D Maxwell–Garnett or Volume Averaging Theory model parameters to the measured reflectance spectra. Both EMAs agreed on the refractive index values but the 2D MGT was more realistic in estimating the film porosity.

By increasing the porosity, we were able to decrease the reflectance and lower the refractive index of silicon. We demonstrated at maximum a 62 % decrease in the reflectance and a 30 % decrease in the refractive index of silicon at 500 nm wavelength using porous films. Optical properties can be further tuned by selecting block copolymers with higher or lower molecular weights or by further optimizing the dry etching process. The proposed method can also easily be extended to suit other substrate materials and wafer sizes thus offering a universal way to manipulate the optical properties of semiconductor and dielectric materials.

ASSOCIATED CONTENT

Supporting Information

Wavelength dependent extinction coefficients of porous silicon films estimated using the 2D Maxwell–Garnett Theory

AUTHOR INFORMATION

Corresponding Author

*Email: hanna.hulkkonen@tut.fi

Author Contributions

The manuscript was written through contributions of all authors. All authors have given approval to the final version of the manuscript**.**

Funding Sources

We acknowledge funding from the Academy of Finland via the projects Photonics QCA (decision no. #263594) and PerforMant (decision no. #284652).

Notes

The authors declare no competing financial interest.

REFERENCES

(1) Peng, J.; Gao, X.; Wei, Y.; Wang, H.; Li, B.; Han, Y. Controlling the Size of Nanostructures in Thin Films via Blending of Block Copolymers and Homopolymers. *J. Chem. Phys.* **2005**, *122*, 1–7.

(2) Yin, J.; Yao, X.; Liou, J. Y.; Sun, W.; Sun, Y. Sen; Wang, Y. Membranes with Highly Ordered Straight Nanopores by Selective Swelling of Fast Perpendicularly Aligned Block Copolymers. *ACS Nano* **2013**, *7*, 9961–9974.

(3) Park, M.; Harrison, C.; Chaikin, P. M.; Register, R. A.; Adamson, D. H. Block Copolymer Lithography : Periodic Arrays of Periodic Arrays of ~10^{11} Holes in 1 Square Centimeter. *Science* **1997**, *276*, 1401–1404.

(4) Xu, T.; Kim, H.-C.; DeRouchey, J.; Seney, C.; Levesque, C.; Martin, P.; Stafford, C. M.; Russell, T. P. The Influence of Molecular Weight on Nanoporous Polymer Films. *Polymer* **2001**, *42*, 9091–9095.

(5) Phillip, W. A.; O'Neill, B.; Rodwogin, M.; Hillmyer, M. A.; Cussler, E. L. Self-Assembled Block Copolymer Thin Films as Water Filtration Membranes. *ACS Appl. Mater. Interfaces* **2010**, *2*, 847–853.

(6) Hilke, R.; Pradeep, N.; Madhavan, P.; Vainio, U.; Behzad, A. R.; Sougrat, R.; Nunes, S. P.; Peinemann, K.-V. Block Copolymer Hollow Fiber Membranes with Catalytic Activity and pH-Response. *ACS Appl. Mater. Interfaces* **2013**, *5*, 7001–7006.

(7) Bang, J.; Jeong, U.; Ryu, D. Y.; Russell, T. P.; Hawker, C. J. Block Copolymer Nanolithography: Translation of Molecular Level Control to Nanoscale Patterns. *Adv. Mater.* **2009**, *21*, 4769–4792.

(8) Salvatore, S.; Demetriadou, A.; Vignolini, S.; Oh, S. S.; Wuestner, S.; Yufa, N. A.; Stefik, M.; Wiesner, U.; Baumberg, J. J.; Hess, O.; Steiner, U. Tunable 3D Extended Self-Assembled Gold Metamaterials with Enhanced Light Transmission. *Adv. Mater.* **2013**, *25*, 2713–2716.

(9) Cummins, C.; Ghoshal, T.; Holmes, J. D.; Morris, M. A. Strategies for Inorganic Incorporation Using Neat Block Copolymer Thin Films for Etch Mask Function and Nanotechnological Application. *Adv. Mater.* **2016**, *28*, 5586–5618.

(10) Ham, S.; Shin, C.; Kim, E.; Ryu, D. Y.; Jeong, U.; Russell, T. P.; Hawker, C. J. Microdomain Orientation of PS-B-PMMA by Controlled Interfacial Interactions. *Macromolecules* **2008**, *41*, 6431–6437.

(11) Durand, W. J.; Carlson, M. C.; Maher, M. J.; Blachut, G.; Santos, L. J.; Tein, S.; Ganesan, V.; Ellison, C. J.; Willson, C. G. Experimental and Modeling Study of Domain Orientation in Confined Block Copolymer Thin Films. *Macromolecules* **2016**, *49*, 308–316.

(12) Thurn-Albrecht, T.; Derouchey, J.; Russell, T. P.; Jaeger, H. M. Overcoming Interfacial Interactions with Electric Fields. *Macromolecules* **2000**, *33*, 3250–3253.

(13) Kim, S. H.; Misner, M. J.; Xu, T.; Kimura, M.; Russell, T. P. Highly Oriented and Ordered Arrays from Block Copolymers via Solvent Evaporation. *Adv. Mater.* **2004**, *16*, 226–231.

(14) Hutchinson, N. J.; Coquil, T.; Navid, A.; Pilon, L. Effective Optical Properties of Highly Ordered Mesoporous Thin Films. *Thin Solid Films* **2010**, *518*, 2141–2146.

(15) Braun, M. M.; Pilon, L. Effective Optical Properties of Non-Absorbing Nanoporous Thin Films. *Thin Solid Films* **2006**, *496*, 505–514.

(16) Pap, A. E.; Kordás, K.; Vähäkangas, J.; Uusimäki, A.; Leppävuori, S.; Pilon, L.; Szatmári, S. Optical Properties of Porous Silicon. Part III: Comparison of Experimental and Theoretical Results. *Opt. Mater. (Amsterdam, Neth.)* **2006**, *28*, 506–513.

(17) Navid, A.; Pilon, L. Effect of Polarization and Morphology on the Optical Properties of Absorbing Nanoporous Thin Films. *Thin Solid Films* **2008**, *516*, 4159–4167.

(18) Sailor, M. Fundamentals of Porous Silicon Preparation. In *Porous Silicon in Practice: Preparation, Characterization and Applications*; Wiley-VCH: Weinheim, Germany, 2012; pp. 1–42.

(19) Yeh, P. *Optical Waves in Layered Media*; Wiley-Interscience: Hoboken, NJ, 2005.

(20) Aspnes, D. E.; Studna, A. A. Dielectric Functions and Optical Parameters of Si, Ge, GaP, GaAs, GaSb, InP, InAs, and InSb from 1.5 to 6.0 eV. *Phys. Rev. B* **1983**, *27*, 985–1009.

(21) Jin, C.; Olsen, B. C.; Luber, E. J.; Buriak, J. M. Nanopatterning via Solvent Vapor Annealing of Block Copolymer Thin Films. *Chem. Mater.* **2017**, *29*, 176–188.

(22) Schubert, E. F.; Kim, J. K.; Xi, J.-Q. Low-Refractive-Index Materials: A New Class of Optical Thin-Film Materials. *Phys. Status Solidi B* **2007**, *244*, 3002–3008.